Journal of Alloys and Compounds 918 (2022) 165434

Contents lists available at ScienceDirect

Journal of Alloys and Compounds

journal homepage: www.elsevier.com/locate/jalcom

Review on the preparation of electrolyte thin films based on cerate-zirconate oxides for electrochemical analysis of anode-supported proton ceramic fuel cells

Mohd Affandi Nur Syafkeena[a], Muhammad Luthfi Zainor[b], Oskar Hasdinor Hassan[c], Nurul Akidah Baharuddin[d], Mohd Hafiz Dzarfan Othman[e], Chung-Jen Tseng[f], Nafisah Osman[a,b,*]

[a] Proton Conducting Fuel Cell Research Group, Faculty of Applied Sciences, Universiti Teknologi MARA, 40450 Shah Alam, Selangor, Malaysia
[b] Physics Department, Faculty of Applied Sciences, Universiti Teknologi MARA, 02600 Arau, Perlis, Malaysia
[c] Faculty of Art & Design, Universiti Teknologi MARA, 40450 Shah Alam, Selangor, Malaysia
[d] Fuel Cell Institute, Universiti Kebangsaan Malaysia, 43600 Bangi, Selangor, Malaysia
[e] Department of Energy Engineering, Faculty of Chemical and Energy Engineering, Universiti Teknologi Malaysia, 81310 Skudai, Johor, Malaysia
[f] Department of Mechanical Engineering, National Central University, Taoyuan 320, Taiwan

ARTICLE INFO

Article history:
Received 31 January 2022
Received in revised form 8 May 2022
Accepted 11 May 2022
Available online 18 May 2022

Keywords:
Proton ceramic fuel cells
Microstructure
Fabrication techniques
Cerate–zirconate electrolyte
Electrochemical performance

ABSTRACT

Proton ceramic fuel cells (PCFCs) are a better alternative to the combustion-based electrical generators because of their high energy conversion efficiency and low carbon emission at relatively low operating temperatures. The electrochemical performance of PCFCs in terms of conductivity, cycling stability, and power density is heavily influenced by the morphological and compositional characteristics of the electrolyte materials. These characteristics can be controlled during the synthesis and fabrication processes. Microstructural modification of the proton ceramic electrolyte can further optimize the electrochemical performance and enhance the efficiency of PCFCs. The well-known electrolyte materials derived from cerate–zirconate ceramic perovskite-type oxides show incredibly high proton conductivity in hydrogen- and/or water-containing atmospheres. This review aims to discuss the influence of electrolyte synthesis and fabrication techniques on the electrochemical properties of PCFCs. Results and findings from different studies are explored and analyzed to examine the effects of grain size, sample density, sintering temperatures, and the addition of metal oxides on the electrolyte performance of PCFCs.

Contents

* Corresponding author at: Physics Department, Faculty of Applied Sciences, Universiti Teknologi MARA, 02600 Arau, Perlis, Malaysia.
E-mail address: fisha@uitm.edu.my (N. Osman).

https://doi.org/10.1016/j.jallcom.2022.165434
0925-8388/

1. Introduction

Solid oxide fuel cells (SOFCs) generate electricity and heat by electrochemically reacting gaseous fuels and reportedly deliver high fuel cell efficiency (up to 80%) depending on the operation conditions and configurations [1–3]. However, high operating temperatures (typically above 800 °C) limit the durability of SOFCs and cause undesirable interfacial diffusion between the electrolyte and electrodes [3–5]. Focusing on a balance between cost, efficiency, and strength, reducing the operating temperatures, and selecting an appropriate cell configuration could address the issues in the SOFC system, although this solution is not that straightforward. Nowadays, reducing high working temperatures has prompted researchers to develop new electrolyte materials. The electrolyte distinguishes the type and mobility of ions in which the selective use of appropriate materials is mandatory for the SOFC to work at a relatively low temperature.

Proton conducting ceramics of perovskite oxide are regarded as promising electrolyte materials to be used in SOFCs at intermediate temperatures in the range of 400–800 °C [6]. These SOFCs are dubbed as proton ceramic fuel cells (PCFCs), and they have distinct advantages over oxygen ion-conducting fuel cells because water is formed at the cathode, thereby increasing electrical efficiency [7–9]. The hydrogen fuel is reduced to a hydrogen ion (H^+) at the anode, and it migrates through the electrolyte toward the cathode (Fig. 1). Moreover, PCFCs exhibit high ionic conductivity and low activation energy (0.4–0.6 eV) compared to the oxygen ion conductor [10–12]. Iwahara et al. were among the first to use perovskite oxide as an electrolyte material with a high proton conductivity below 800 °C [13]. The general formula for this perovskite-type oxide is ABO_3 with an ideal cubic symmetrical structure, where the A-site cation is coordinated with 12 oxygen ions and the B-site cation forms a BO_6 octahedron when complexing with six oxygen ions. H^+ ions require lower activation energy to transport through perovskite crystal structures because of their small ionic radius and the absence of an electron cloud compared with oxygen ions (O^{2-}). Considerable attention has been paid to improve well-established ABO_3 materials, such as cerate–zirconate oxides, for the electrolyte, but enhancements concerning quality, duplicability, and economic process still need to be considered. From a wide range of ceramic proton conductors, the barium cerate–zirconates can offer a significant advantage to attain these goals.

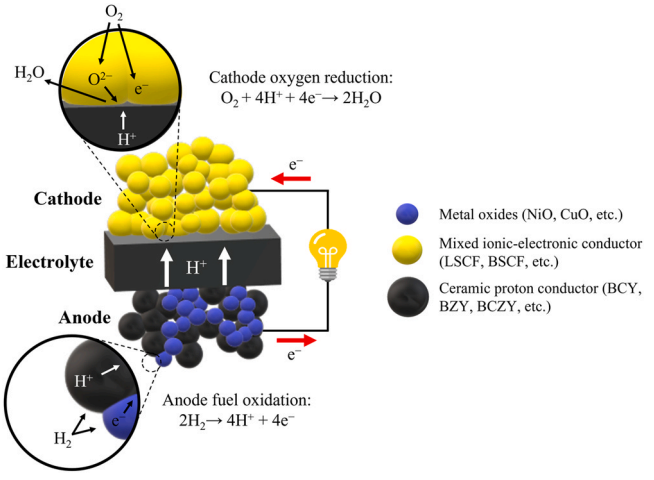

Fig. 1. A schematic diagram of solid oxide fuel cell components based on proton conductor electrolyte.

Fig. 2 shows the evolution of proton-conducting electrolytes based on perovskite-type oxide (focusing on the cerate–zirconate ceramics) over time. Takahashi and Iwahara [14] did pioneering work on perovskite-type oxides, which was continued by Iwahara et al. [15,16] in the following years for application in SOFCs at 600–1000 °C using doped strontium cerate oxide ($SrCe_{0.95}Yb_{0.05}O_{3-\alpha}$) and doped barium cerate oxide ($BaCeO_3$). Wienströer and Wiemhöfer prompted further research using doped barium cerate with partial substitution of zirconium [17]. Consequently, researchers have taken extensive efforts to optimize and explore the electrochemical properties of proton-conducting, acceptor-doped barium cerate ($BaCeO_3$) and zirconate ($BaZrO_3$) materials, including their structural and chemical stability, transport properties, and conductivity. Tseng et al. [18] demonstrated that optimization doping at the A-site of perovskite oxide $Ba_{0.9}K_{0.1}Ce_{0.6}Zr_{0.2}Y_{0.2}O_{3-\delta}$ could be a promising electrolyte for SOFC operations at intermediate temperatures. Recent studies on proton-conducting electrolytes have been heading toward dual ion-conducting electrolytes, as demonstrated by Zhou et al. [19] who used $BaZr_{0.1}Ce_{0.7}Y_{0.1}Yb_{0.1}O_{3-\delta}$ to conduct proton and oxygen ions. In another study, Rajendran et al. [20] investigated tridoped $BaCe_{0.5}Zr_{0.2}Y_{0.1}Gd_{0.1}Pr_{0.1}O_{3-\delta}$ to improve the sinterability issues while improving the chemical stability and proton conductivity.

The electrolyte film microstructure also influences the electrochemical properties of an anode-supported single cell [21,22]. Particle size distribution, particle shape, and relative density can be influenced by synthesis methods, contributing to the final microstructure of the film. Preparation conditions, such as the addition of a sintering aid and sintering conditions (sintering techniques, temperature, and time), also play a significant role in determining the final microstructure of the prepared sample. However, from a review of the publishing rate and patent search through Web of Science, few published studies [23,24] have focused on the aforementioned conditions during the fabrication of a dense electrolyte thin film for doped $BaCeO_3$, $BaZrO_3$, and $Ba(Ce,Zr)O_3$ since 2017. Thus, in the present study, the performance of proton ceramic electrolytes with various fabrication methods, sintering processes, and grain sizes is investigated. These external factors can manipulate the microstructure of the electrolyte films without changing the electrolyte perovskite structure. We elucidated the benefits and drawbacks of each method for improving material properties of the anode. The performance of the PCFC is significantly induced by the dense electrolyte microstructure. Therefore, a comprehensive review of the preparation conditions is indispensable.

2. Effects of physical properties (nanosize and grains) on electrochemical performance

However, from a review of the publishing rate and patent search through Web of Science, few published studies [23,24] have focused on the aforementioned conditions during the fabrication of a dense electrolyte thin film for doped $BaCeO_3$, $BaZrO_3$, and $Ba(Ce,Zr)O_3$ since 2017. Thus, in the present study, the performance of proton ceramic electrolytes with various fabrication methods, sintering processes, and grain sizes is investigated. These external factors can manipulate the microstructure of the electrolyte films without changing the electrolyte perovskite structure. We elucidated the benefits and drawbacks of each method for improving material properties of the anode. The performance of the PCFC is significantly induced by the

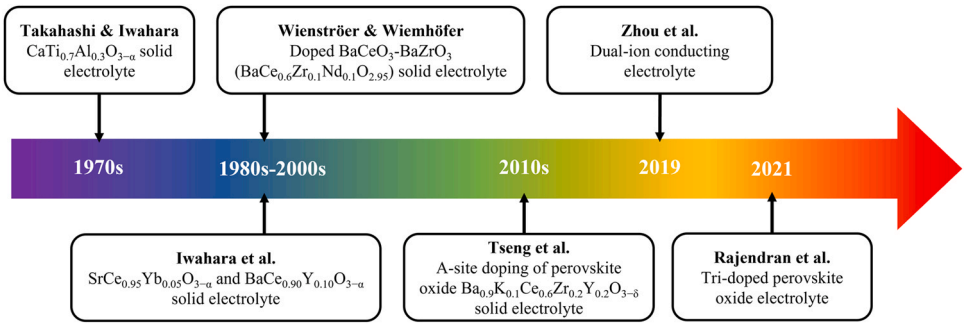

Fig. 2. Overview of the timeline for proton ceramic electrolyte based on perovskite-type oxide.

dense electrolyte microstructure. Therefore, a comprehensive review of the preparation conditions is indispensable.

Of all the methods used for the synthesis of electrolyte powder, wet chemical methods, such as sol–gel, Pechini, gel casting, and combustion route, lead to the successful synthesis of compositionally homogeneous powders with high crystallinity and high phase purity at a relatively low temperature [25,26]. Several researchers have produced nanosized doped cerates [27–29]. For instance, a modified sol–gel Pechini method was found to be appropriate for obtaining nanosized powders using ethylenediaminetetraacetic acid as a chelating agent; this method ensured the homogeneous mixing of metallic cations at a molecular level and improved powder morphology by lowering calcination temperatures. Mazlan et al. [30] further modified the sol–gel method by using surfactants to reduce calcination temperature and decrease the particle size to the nanoscale. They stated that there was a weak electrostatic interaction because of the lone pair of oxygen electrons in the nonionic surfactant, thereby helping to prevent agglomeration between particles during the synthesis process.

The reduction of powder grain size to nanostructures was performed to lower the sintering temperatures of the electrolytes and consequently reduce the loss of BaO via evaporation observed at high temperatures. Moreover, previous studies have emphasized that dense electrolytes with excellent properties can be easily obtain by sintering uniform nanopowders as compared to sintering irregular micrometer-sized powders. Wang et al. [31] prepared 30-nm particles of $BaZr_{0.1}Ce_{0.7}Y_{0.1}Yb_{0.1}O_{3-\delta}$ (BZCYYb) precursors by coprecipitation. A dense BZCYYb sample with an average grain size of 184 nm was obtained using a two-step sintering (TSS) process, whereas BCZYYb with submicron grains of 445 nm was produced by conventional sintering. The fine grains of BZCYY using the TSS process showed enhanced electrical conductivity and reduced ohmic and polarization resistances; they reached a power density of 349 mW cm^{-2} at 700 °C. A recent study by Min et al. [32] reported similar findings involving a cell with nanograin electrolytes that was obtained from nanoparticles via coprecipitation. The single cell exhibited high open-circuit voltage (OCV) and maximum power density (1.0 V and 300 mW cm^{-2}) at 700 °C, improving the electrochemical reaction at the anode–electrolyte interface and preventing gas crossover. These results suggested that adjusting the final microstructure by applying nanoparticles was crucial for obtaining fine grains, which optimized the microstructure and enhanced the electrochemical performance of electrolytes in the SOFC system.

In terms of electrical conductivity, Ma et al. [33] deduced that higher protonic conductivity of nanograined $BaCe_{0.5}Zr_{0.4}Y_{0.1}O_3$ (BCZY) is associated with its nanostructure, which helps obtaining higher proton conductivity than similar perovskite membranes [13]. However, the BCZY membrane is verified to be a mixed conductor, with a high electronic ratio of protonic between 700 °C and 800 °C. As the testing temperature dropped below 500 °C, the protonic conductivity prevailed. A similar conclusion was reached by Park et al. [34], who tested nanograined $BaZr_{0.9}Y_{0.1}O_3$ (BZY) at temperatures > 200 °C. They found that nanograined BZY had enhanced protonic conductivity compared to that of the micron-sized BZY grains, possibly due to the hydration and dehydration of water adsorbed to the grain boundary. The study also demonstrated that the protons in nanograined BZY are transferred using the "grain route" at low temperatures, because resistivity at the grain boundary is still higher than that in the grain. Nanoscale materials have a higher grain boundary volume. We assumed that nanoscale grains are more selective in terms of testing temperature and are suitable for use at intermediate to low temperatures (400–100 °C).

However, there is a limit to which the extent grain size will benefit conductivity. Cervera et al. [35] studied the effect of grain size on the conductivity of $BaZr_{0.75}Sc_{0.25}O_{3-\delta}$ (BZY) fabricated at 350 °C, 800 °C, and 1250 °C, with average grain sizes of 8.9, 15.9, and 68.5 nm, respectively, using transmission electron microscopy. The highest conductivity was achieved for the sample with an average grain size of 68.5 nm (1.27×10^{-3} S cm^{-1} at 500 °C). The observed conductivity for the fine-grained electrolyte is comparable to that reported for the benchmark BZY with nanometer and submicrometer grains. Based on these data, the findings support the notion that the grain size influences conductivity and smaller grains do not necessarily provide good conductivity. As mentioned above, the sample with 8.9 nm grains contained traces of hydrated oxides and hydroxides that possibly existed as a thin coating on the surface of the grains and led to low conductivity. Similar findings regarding the effects of different grain sizes of the oxide ion were obtained. A samaria-doped ceria electrolyte showed enhancement in ionic conductivity and an increase in the grain boundary ionic diffusivity with decreasing grain size [36].

3. Thin-film fabrication conditions

The fabrication method is crucial to significantly determine a material's structural and morphological characteristics. Technical strategies are essential in fabricating ceramic components to achieve better compactness and finer grain sizes that contribute to the electrical, thermal, and mechanical properties. In particular, thin-film electrolytes are used in SOFCs to reduce ohmic resistance, leading to the increase in power at the external useful load with a decrease in operating temperature. Thin-film electrolytes have advantages over thick films or bulk materials in terms of the following: (i) reducing oxygen ions or proton traveling distance, because resistance is inversely proportional to conductor length; (ii) producing grain structures that are less resistive, such as columnar grain structures; (iii) controlling the nanocrystalline microstructure of thin films, which enables fine-tuning of electrical conductivity; and (iv) depositing films with large interfacial areas, as the power output is also proportional to interfacial area. Thus, it is reasonable to reduce the thickness of solid electrolytes to 10–20 µm while maintaining a gas-tight characteristic feature. A study by Park et al. [37]

demonstrated the effect of electrolyte thickness and operating temperature on the performance of SOFCs in terms of heat and mass transfer characteristics. As expected, the maximum power density increased with decreasing electrolyte thickness, and the difference became significant when the current density increased with varying electrolyte thicknesses at a fixed temperature. Thinner electrolytes are beneficial for volumetric power density due to the lower ohmic loss.

Dip-coating, spin-coating, and screen-printing methods are categorized as colloidal methods. These methods require the preparation of liquid precursors (frequently termed as slurry or ink) before deposition onto an anode substrate. A typical liquid precursor is composed of a solid (electrolyte powder), an inorganic solvent, and a binder. The dip-coating method is suitable for a variety of geometric shape cells [38] and is commonly selected for tubular SOFC fabrication [39–41], whereas several methods have been reportedly used for planar SOFC fabrication [42–44]. The stages in the dip-coating process include immersion, start-up, deposition, drainage, and evaporation. The electrolyte film thickness can be controlled by the number of coatings completed; after each coating, the cell undergoes a drying process. Although a thinner electrolyte layer is suitable for electrochemical performance, it has a high possibility of increasing the chances of gas leakage. Lei et al. [45] conducted a study of the dip-coating method for fabricating anode-supported cells; their findings revealed that a thinner electrolyte layer results from a low-viscosity slurry and leads to poor electrolyte/anode contact.

The spin-coating method is an inexpensive and straightforward batch production process for electrolyte thin-film fabrication. It is a process that involves spinning liquid precursors on an anode substrate at a high speed. The spin-coating process involves the following steps: (1) the deposition of slurry on a flat anode substrate; (2) the spin-up of the slurry during spinning; (3) the spin-off of excess slurry with decreasing spinning speed; and (4) the evaporation of the slurry. The spin-coating method has good reproducibility to yield dense electrolytes with controlled thickness [46]. Another study revealed an OCV value of 1.0–1.1 V for a 14-μm electrolyte layer fabricated by the spin-coating method at 600 °C [47]. Other works on the fabrication of the electrolyte by the spin-coating method proved the reproducibility of obtaining gas-tight membranes with high OCV values [48–50]. However, this method is limited in scalability and leads to slurry/ink wastage during the spinning process.

The final thickness of the film relies on the properties of liquid colloids, such as solid content, binder percentage, and viscosity, and spinning processes, such as rotational speed and time. One significant property of this method is the use of high spinning speeds (> 3000 rpm) to effectively acquire a dense electrolyte layer because a lower spinning speed will leave more pores (from the binder or dispersant) after sintering of the electrolyte [51]. If the electrolyte layer is too thin, some changes are made in the spin-coating parameters, such as selecting a lower spinning speed, reducing the spinning time during a high-speed step, and/or reducing the amount of binder/increasing the amount of solid content. In contrast, if the final electrolyte layer is too thick, then the following steps can be performed: selecting a higher spinning speed, increasing the spinning time during a high-speed step, and/or increasing the amount of binder/reducing the amount of solid content. The insufficient dispensing volume of electrolyte slurry/ink before the spinning process may result in the insufficient coating of the entire anode substrate by the final electrolyte layer.

Screen printing is another versatile and straightforward approach for producing thin electrolyte films. This method uses an electrolyte ink, a squeegee, and a screen mesh with desired aperture and template size and can produce high-quality electrolyte films with thicknesses in the range of 10–100 μm. According to Baharuddin et al. [52], who used screen printing, the final films are highly dependent on a wide range of factors, such as screen-printing speed, screen mesh aperture selections, angle of the squeezer, and the rheology of the ink. Hossain et al. [53] fabricated a Ni-BCZYS|BCZYSZn|LSCM cell using a screen printing method for electrolyte and cathode layers. The screen printing process is reliable for achieving a dense electrolyte film with an OCV surpassing 1.01 V and a maximum power density of 420 mW cm^{-2} at 700 °C. A study by Choi et al. [54] reported that using a screen-printed BZYCu electrolyte followed by sintering at 1500 °C for 3 h resulted in films with thicknesses of 10 μm and OCV values of 0.98 V at 650 °C. Using the same method, a single cell with a BCZYSm electrolyte film fabricated by Meng et al. [55] exhibited an OCV of 1.0 V and a power density of 200 mW cm^{-2} with a thickness of 25 μm.

Other methods, such as electrochemical vapor deposition (EVD), electrostatic slurry spray deposition, and pulsed laser deposition (PLD) are advanced processes that can deposit dense and high-quality coatings ranging from submicrometer to tens of nanometer scales. These methods are called physical vapor deposition methods because they use a high-energy source for evaporation of the electrolyte material. Subsequently, a reaction between the metal atoms and an appropriate reactive gas occurs while transporting the vapor. Finally, deposition of the material occurs on the substrate. Bae et al. [56] fabricated an approximately 1.5-μm thick BCZY film on an anode-supported single cell, which is the thinnest proton-conducting electrolyte film ever fabricated via the PLD method. This cell achieved a very low ohmic resistance of 0.15 Ω cm^2, which is proportional to the electrolyte thickness, an OCV of 1.03 V, and maximum power density of 500 mW cm^{-2} at 600 °C. Moreover, Konwar et al. [57] showed similar results on the 3-μm thick BCZYYb electrolyte film fabricated via EVD. Despite producing extremely thin electrolyte films that are advantageous for electrochemical performances, physical vapor deposition is a complex and expensive technique and is, therefore, not widely used [58]. Fig. 3 illustrates the abovementioned electrolyte film production procedures.

Table 1 outlines the most widely adopted electrolyte film production procedures for anode-supported SOFC construction. Uniaxial pressing, spin coating, dip coating, screen printing, and tape casting are often used for laboratory-scale manufacturing due to their low cost and ease of use. Uniaxial pressing is a procedure commonly used in conjunction with the cosintering process of anode/electrolyte membranes to generate electrolyte thickness values of > 20 μm. Based on previous studies [59–61], the electrolytes fabricated via uniaxial pressing have successfully obtained dense layers with OCV values of approximately 1.0 V, which are near the theoretical values for proton-conducting electrolyte materials. OCV represents the maximum electrical potential of a sample when no load is applied (open circuit). However, many recent studies have shown that the copressing technique can achieve an electrolyte thickness of 10–15 μm [62]. Thus, uniaxial pressing can be regarded as the easiest and most economical method for obtaining good contact between the thin electrolyte layer and the anode substrate while maintaining a dense electrolyte structure.

3.1. Sintering process

Sintering involves applying heat to a sample to reduce its porosity and increase its strength while improving the electrical conductivity, translucency, and thermal conductivity. Generally, a proton ceramic electrolyte requires a processing temperature of > 1100 °C to form the required single-perovskite phase powder and a sintering temperature of over 1600 °C to obtain optimal dense bulks/films. However, the usual powder technology processes for sintering solid oxide electrolytes are energy-intensive due to the high temperatures and long sintering period (10–20 h) needed, thereby resulting in undesirable reactions with the electrode materials, element evaporation, or undesired phase formation [72].

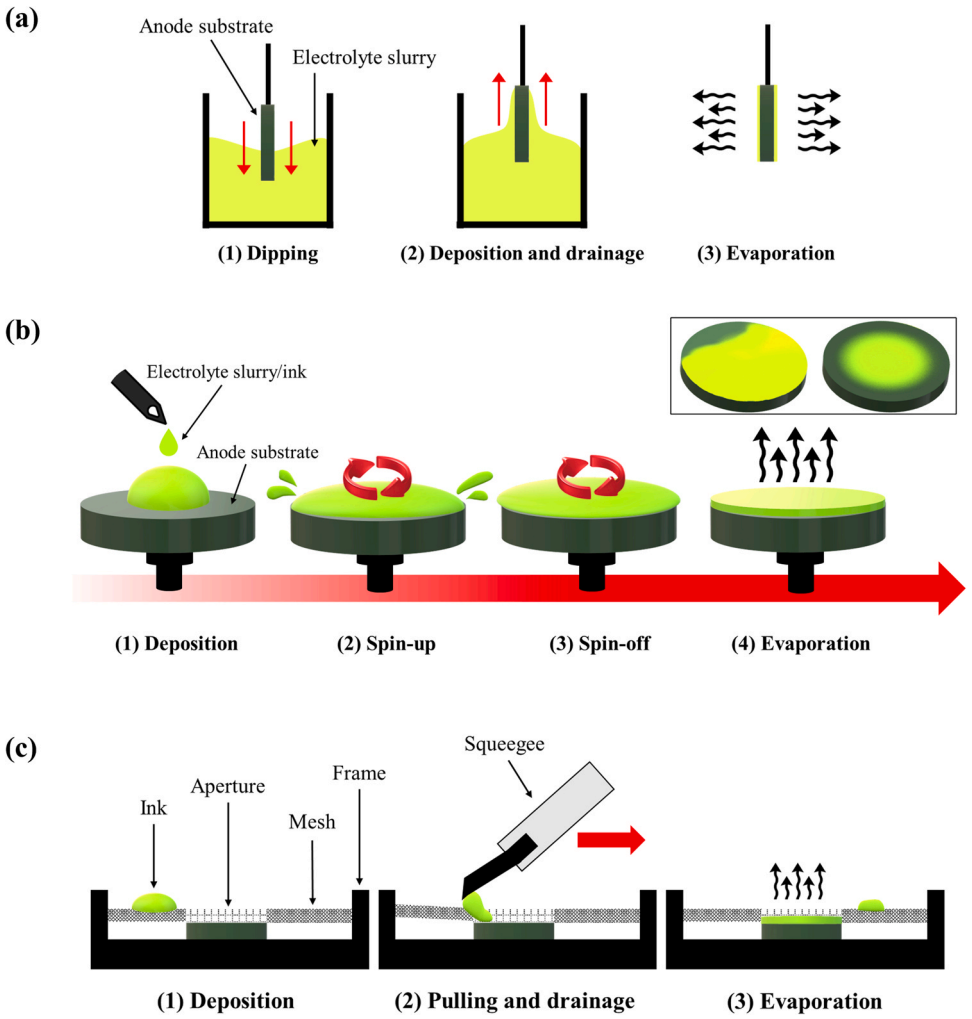

Fig. 3. Illustrations of various processes to fabricate electrolyte film on anode substrate via (a) dip coating method, (b) spin coating method with indication of inadequate slurry deposition (insert figure), and (c) screen-printing method.

Hence, considerable efforts have been made to reduce the sintering temperatures of these materials. In addition, the choice of sintering profiles plays a crucial role in adjusting the final microstructure, especially the grain size distributions and densities of the ceramics.

Previous studies obtained a refined microstructure for the ceramic samples by tuning the sintering temperature and time prior to the emergence of advanced techniques, such as spark-plasma sintering and high-temperature microwave sintering, which involved the rapid heating of samples to high temperatures to prevent or suppress grain growth [73]. Sintering methods are classified into conventional and unconventional sintering based on the sintering temperature (Fig. 4). Conventional sintering is a traditional heating method that uses high temperatures without applying pressure, such as one-step sintering (only one temperature), TSS (two different temperatures), cosintering, or metal oxide assisted sintering. Unconventional sintering compacts the powder by using pressure, gas, or sophisticated heating mechanisms (such as cold pressing, hot pressing, spark-plasma, or microwave sintering).

3.2. TSS method

An economical alternative in preparing dense electrolyte bulk/film is the TSS method. The earliest TSS method applied to ceramic materials of alumina (Al_2O_3) and magnesium (MgO) powders was developed by Chu et al. [74] in the 1990 s. In this method, the first temperature (T_1) is lower than the second temperature (T_2). TSS can reduce the sintering time at peak temperature to several minutes followed by sintering at a lower temperature for several hours. The applied temperature allows refinement of the microstructure, and dense samples are obtained after a short soaking time at high sintering temperatures. Huang et al. [75] implemented the method to obtain dense silicon nitride (Si_3N_4). In addition to obtaining a dense electrolyte layer, another prominent feature of films sintered via the TSS is increased grain growth. Thus, the TSS method is useful for obtaining samples with large grains after sintering. Sample with large grains reduce the grain boundary resistance and are favorable for increasing the cell's total conductivity. Moreover, the TSS method provides benefits in terms of the alleviation of BaO evaporation while simultaneously achieving the desired relative density. This TSS approach was later acknowledged as the conventional TSS method, and Chen and Wang [76] devised a newly modified TSS method that is described below.

In the modified TSS technique, T_1 is set to a higher temperature as compared to T_2. The first-stage high-temperature step helps in eliminating supercritical pores, whereas the second-stage low-temperature sintering suppresses grain growth. Grain boundary migration is suppressed at high temperatures while allowing grain boundary diffusion at low temperatures. This method has been successfully applied to obtain a dense electrolyte film with fine microstructures at nanosized grains, including Y_2O_3, SiC [76], and BZCYYb [31,77]. Using TSS to sinter thin-film BCZYYB yielded higher sinterability than the conventional sintering method. The modified

Table 1
The comparative analysis of electrochemical properties of planar anode-supported cells with respective electrochemical performances at 600 °C (unless stated otherwise).

Methods	Properties	Electrolyte			OCV (V)	Power density (mW cm^{-2})	Ref.
		Nominal composition	h (μm)	R_{ohm} (Ω cm^2)			
Dip-coating	• Batch processing	$BaZr_{0.8}Y_{0.2}O_{3-\delta}$	25	3.24	0.97	55	[42]
	• Time consuming	$BaZr_{0.1}Ce_{0.7}Y_{0.2}O_{3-\delta}$	40	–	0.8–0.9	668	[43]
	• Average scalability	$BaCe_{0.7}Zr_{0.1}Y_{0.1}Yb_{0.1}O_{3-\delta}$	10	0.58	~1.05	150	[44]
Tape calendaring/casting	• High scalability	$BaCe_{0.5}Zr_{0.3}Y_{0.2-x}Yb_xO_{3-\delta}$	25	1.04	1.01	140	[63]
	• Industrialized	$BaCe_{0.5}Zr_{0.3}Dy_{0.2}O_{3-\delta}$	30	0.86	1.06	290 (550 °C)	[64]
	• Efficient	$BaCe_{0.5}Zr_{0.3}Y_{0.2}O_{3-\delta}$ +CuO	35	0.8–1.2	1.14	174	[65]
	• Simple						
Uniaxial pressing	• Single processing	$BaZr_{0.4}Ce_{0.4}Y_{0.2}O_{3-\delta}$	20	~1.40	~1.0	116	[59]
	• Low cost and easy to operate	$BaZr_{0.8}Y_{0.2}O_{3-\delta}$ + CuO	25	~1.5	~0.99	72	[60]
		$BaCe_{0.8}Sm_{0.1}Y_{0.1}O_{3-\delta}$	~20	–	0.99	220	[61]
	• Limited in scalability						
	• Time consuming						
Spin-coating	• Batch processing	$BaZr_{0.1}Ce_{0.7}Y_{0.1}Yb_{0.1}O_{3-\delta}$ + NiO	10	~0.30	1.0	250–300	[50]
	• Low cost and easy to operate	$BaZr_{0.1}Ce_{0.7}Y_{0.1}Yb_{0.1}O_{3-\delta}$	14	–	1.0–1.1	570	[47]
		$BaZr_{0.6}Ce_{0.2}Y_{0.2}O_{3-\delta}$	30	0.58	1.08	336	[49]
	• Average in scalability	$BaCe_{0.4}Zr_{0.4}Y_{0.2}O_{3-\delta}$	~5	0.769	1.03	102	[48]
	• Ink/slurry wastage						
Screen printing	• Cost-effective process	$BaCe_{0.6}Zr_{0.2}Y_{0.15}Sm_{0.05}O_{3-\delta}$	39	–	1.01	420 (700 °C)	[53]
	• High scalability	$BaZr_{0.84}Y_{0.15}Cu_{0.01}O_{3-\delta}$	10	2.0–3.0	0.98	28.2 (650 °C)	[54]
	• Moderate ink/slurry wastage	$BaCe_{0.7}Zr_{0.1}Y_{0.07}Sm_{0.13}O_{3-\delta}$	25	~0.58	~1.0	200	[55]
Electrostatic slurry spray deposition	• High deposition rate	$BaCe_{0.5}Zr_{0.35}Y_{0.15}O_{3-\delta}$	~8	0.31	1.05	231	[66]
	• Produces a very thin layer						
Electrochemical vapor deposition	• High cost	$BaZr_{0.1}Ce_{0.7}Y_{0.1}Yb_{0.1}O_{3-\delta}$	3	0.15	1.0–1.1	560	[57]
	• Produce very thin layer	$BaZr_{0.2}Ce_{0.7}Y_{0.1}O_{3-\delta}$	4	0.12	1.05	910	[67]
	• Industrialized						
	• High efficiency						
Pulse laser deposition	• High cost	$BaCe_{0.55}Zr_{0.3}Y_{0.15}O_{3-\delta}$	~1.5	0.15	1.03	~500	[56]
	• Produce very thin layer						
	• High efficiency						
Wet powder spraying/spray coating	• Industrialized	$BaZr_{0.1}Ce_{0.7}Y_{0.1}Yb_{0.1}O_{3-\delta}$	4	0.303	1.105	418	[68]
	• High scalability	$BaCe_{0.85}Y_{0.15}O_{2.925}$	10	0.6–0.7 (700 °C)	0.95 (750 °C)	–	[69]
	• Moderate reliability						
		$Ba_{0.98}Ce_{0.6}Zr_{0.2}Y_{0.2}O_{3-\delta}$	10–15	–	~1.1	493	[70]
		$BaZr_{0.1}Ce_{0.7}Y_{0.2}O_{3-\delta}$	17	0.68	1.02	177	[71]

Abbreviations: electrolyte thickness (h), Ohmic resistance (R_{ohm}).

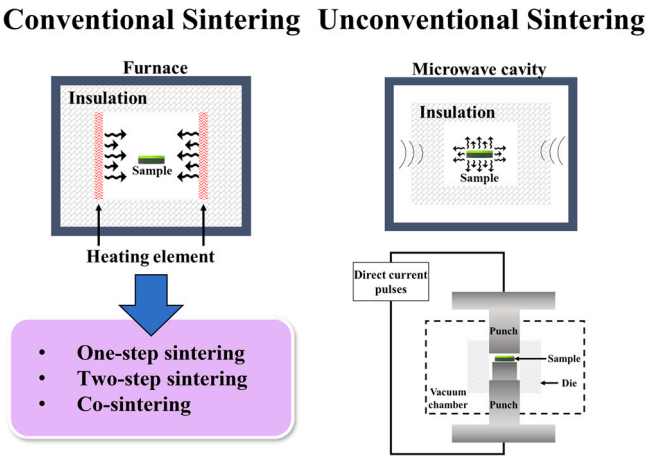

Fig. 4. Schematic diagrams of conventional and unconventional sintering based on the sintering temperature.

TSS technique facilitates the formation of dense microstructures at lower sintering temperatures, resulting in the increased performance of the cell. The maximum power output of the cells fabricated using the TSS method reached 349 mW cm^{-2} because of the reduced ohmic and polarization resistances; this value was a significant improvement from 172 mW cm^{-2} at 700 °C for the conventionally sintered cells. These advancements suggest that it is favorable to use the modified TSS method for preparing barium cerate-based dense proton-conducting ceramics and their anode-supported SOFCs.

3.3. Cosintering method

Cosintering is another simple alternative technique to achieve dense electrolyte films. Generally, this method begins with the fabrication of the anode substrate, which is then coated with an electrolyte layer either in powder or slurry form. Ding and Xue [78] fabricated an anode-supported BCZYYb bilayer using a dry-pressing technique. The BCZYYb powder was evenly distributed onto the anode substrate and copressed before sintering at 1450 °C for 5 h. Lin et al. [79] assembled an anode-supported BCZYZn bilayer via dry-pressing. The BCZYZn powder was copressed onto a green anode substrate and cosintering was applied at 1250 °C for 5 h. When the electrolyte is used in powder form during copressing, the dry-press pressure for the electrolyte is customarily adjusted higher than that of the anode substrate in the cosintering process, which helps in the formation of a dense electrolyte film microstructure after sintering. If electrolyte slurry is used, then a spin coater is usually adopted. The thickness of the electrolyte film is determined through the rotation speed and time of the spin coater. As mentioned earlier, the typical rotation speed is set at more than 3000 rpm to produce dense electrolyte films.

The effectiveness of the cosintering process lies in the anode-supported configuration, which facilitates film electrolyte sintering. Ni diffusion from the anode may promote densification of the electrolyte layer, thus lowering the sintering temperature. The concept is similar to using metal oxides, such as nickel oxide, zinc oxide, or copper oxide, as sintering additives for electrolyte membranes, as discussed in Section 5. In addition, because of the simplicity and effectiveness of the TSS and cosintering methods, a novel two-step cosintering method has been introduced by Wang et al. [80], which

Table 2
Summary of anode/electrolyte bilayer fabrication using the cosintering method (with respective pressing pressures if stated).

Material for anode/electrolyte bilayers	Fabrication method for the bilayers		T (°C)	h (μm)	Cell performance		Ref.
	Anode	Electrolyte			OCV (V)	Power density ($mWcm^{-2}$)	
NiO-$Ba(Zr_{0.84}Y_{0.15}Cu_{0.01})O_{3-\delta}$/BZY	Dry-press (200 MPa)	Screen printing	1500 (5 h)	~10	0.95 (650 °C)	28.2 (650 °C)	[54]
NiO-BZY/BZY	Dry-press	Dry-press	1400 (6 h)	~25	0.99 (700 °C)	141 (700 °C)	[60]
NiO- $BaCe_{0.8}Sm_{0.1}Y_{0.1}O_{3-\delta}$/BCSY	Dry-press	Dry-press	1400 (6 h)	~20	0.99 (600 °C)	220 (600 °C)	[61]
NiO-$BaZr_{0.75}Y_{0.2}Pr_{0.05}O_{3-\delta}$/BZYP	Dry-press	Dry-press	1450 (10 h)	~20	0.93 (600 °C)	124 (600 °C)	[87]
NiO-$BaCe_{0.95}Tb_{0.05}O_{3-a}$/BCTb	Dry-press (3 MPa)	Dry-press (10 MPa)	1450 (5 h)	11	0.99 (700 °C)	753 (700 °C)	[88]
NiO-BCZYYb/BCZYYb	Dry-press (200 MPa)	Dry-press (250 MPa)	1400 (5 h)	15	1.006 (700 °C)	452 (700 °C)	[78]
NiO-BZY/BZY	Dry-press (150 MPa)	Dry-press (200 MPa)	1400 (5 h)	30	0.90 (700 °C)	172 (700 °C)	[89]
NiO-$BaCe_{0.5}Zr_{0.3}Y_{0.16}Zn_{0.04}O_{3-\delta}$/BCZYZn	Dry-press (200 MPa)	Dry-press (250 MPa)	1250 (5 h)	30–40	1.0 (700 °C)	236 (700 °C)	[79]
NiO-BZY/BZY	Dry-press (392 MPa)	Spin-coating	1500 (5 h)	10–15	–	–	[90]
NiO-BZYb/BZYb				10–20	–	–	
NiO-BCZY/BCZY	Dry-press	Dry-press	1450 (5 h)	12	0.95–1.0(700 °C)	175–200(700 °C)	[91]
NiO-BCZY/$BaCe_{0.7}In_{0.2}Yb_{0.1}O_{3-\delta}$	Dry-press	Dry-press (300 MPa)	1450 (5 h)	~30	0.963 (700 °C)	280 (700 °C)	[92]

Abbreviations: cosintering temperature (T), electrolyte thickness (h).

lowers the cosintering temperature of the anode–electrolyte bilayer and restricts the particles' grain growth to obtain a fine-grained dense electrolyte and ultrafine anode particles with high porosity. A dense $Ba_3Ca_{1.18}Nb_{1.82}O_{9-\delta}$ electrolyte film and a porous anode support with fine particle sizes were obtained at a significantly reduced temperature of 1300 °C. These are cost-effective fabrication methods that can be used to produce reliable SOFCs. A summary of the literature on producing anode-supported SOFCs by cosintering as well as the cell performance, which is affected by the sintering conditions of the cell, are shown in Table 2.

3.4. Unconventional sintering methods

A more technologically advanced method to obtain dense electrolyte films, including spark-plasma sintering and high-temperature microwave sintering, has been recently developed. The material's microstructure is significantly altered because of the difference in heat distribution in each of these sintering methods. The spark-plasma sintering (SPS) method is a high-speed powder consolidation technique that uses uniaxial force and a pulsed (on-off) direct electrical current under low atmospheric pressure based on an electrical spark discharge phenomenon induced by a high-energy, low-voltage pulse direct current that momentarily creates spark plasma (usually at temperatures > 1300 °C, sintering time 5–10 min) in the fine spaces between the particles. The SPS method allows exceptionally high heating and cooling rates, thereby enhancing densification over grain growth and promoting diffusion mechanisms [81]. SPS was applied at 1350 °C for 5 min to obtain a pore-free $BaZr_{0.5}Ce_{0.3}Y_{0.2}O_{3-\delta}$ electrolyte film with an excellent protonic conductivity at 600 °C [73]. Similar work by Wang et al. [82] employed SPS to produce a $BaZr_{0.9}Y_{0.1}O_{3-\delta}$ film at 1400 °C. Simonenko et al. demonstrated that SPS can be used for obtaining a dense $BaCe_{0.9-x}Zr_xY_{0.1}O_{3-\delta}$ film at a surprisingly low temperature of 900 °C, which is one of the lowest recorded temperatures to sinter cerate–zirconate-based electrolytes [83]. Therefore, the SPS method is beneficial because of the low sintering temperature, short holding time, no precompaction, and short sintering time. An additional advantage of the technique is the production of fine-sized grains that help increase the electrochemical conductivity of the cell [33].

Microwave sintering is another alternative method that is used to obtain dense electrolyte films at a short processing time with improved microstructure and electrochemical properties. The heat distribution process begins with the inner surface of the materials and progresses to the outer surface before the entire surface volume is heated, which allows the efficient and uniform transfer of energy [84]. Xu et al. [85] used this method for preparing BCZY electrolyte membranes, allowing the membrane to densify at 1200 °C, a considerably low temperature for sintering highly dense barium cerate–zirconate-based oxide. The same study reported that the conventionally sintered BCZY remained porous after thermal treatment at the same temperature. Lowering the sintering temperature to some extent enables a more homogeneous elemental distribution and lesser Ba evaporation than the conventional sintering process, which uses a furnace, thereby leading to higher electrolyte conductivity. Wang et al. [86] used a combination of cosintering and microwave sintering to produce desirable electrolyte densification with a cathode–electrolyte interface that shows good contact, which is crucial for improving fuel cell performance. At 700 °C, the cell produced 449 mW cm^{-2}, which was greater than the conventional cosintering method. Polarization resistance decreased because the cathode was properly adhered to the electrolyte layer.

In summary, conventional sintering procedures are time consuming and impractical for large-scale SOFC production, but a minor reduction in sintering time can be accomplished using TSS, cosintering, or sintering aids. High sintering temperatures could lead to element evaporation of the material and elemental diffusion, which are detrimental to the electrical performance of the proton-conducting oxides. In addition, grain growth inhibition could not be regulated because of the materials' uneven heat distribution during the sintering process. Nonetheless, most researchers prefer using conventional sintering because it is a straightforward and cost-effective approach. However, unconventional sintering procedures offer much lower sintering temperature with rapid sintering, which enables a more homogeneous elemental distribution. The application of these sophisticated procedures provides an efficient and uniform transfer of energy, which is suitable for the preservation and densification of nanocrystalline features in the ceramic material; however, one drawback is the use of expensive machines that require extra care. Based on the abovementioned discussion, in terms of practical application and the cost, efficiency, and repeatability of sintering, unconventional sintering methods—such as SPS and microwave sintering—could provide better solutions in the processing of proton-conducting ceramics of perovskite oxide.

3.5. Sintering additives

Most cerate electrolytes with high relative density (such as $BaCeO_3$ and $SrCeO_3$) are relatively simple to fabricate [13], whereas Zr-containing electrolytes typically require sintering at extremely high temperatures [93]. High-temperature sintering causes severe problems, such as extreme thermal conditions, material deterioration, and potential changes in the chemical compositions of the electrolytes [94]. Several studies suggested that high-temperature sintering caused evaporation or segregation from the crystal lattice of component elements, such as Ba and Y, leading to the destruction of the electrical conductivity (decreased by two orders of magnitude) of $BaZr_{0.8}Y_{0.2}O_{3-\delta}$ [95,96]. Han et al. [97] verified the existence of an impurity: Y_2O_3 was present in the BZY electrolyte because of

extreme temperature conditions, and it potentially blocked the pathway of proton transportation, leading to the regression of conductivity.

The limitation of high-temperature sintering can be overcome by adding a small amount of a sintering additive to improve the microstructure properties of the electrolytes. The additive in the electrolyte material composition serves as a "glue" that benefits the materials' sinterability and improves the performance of ceramic materials by altering their densifying behavior [98,99]. Previous studies have shown that adding sintering additives to ceramic systems causes particle shrinkage or growth, dimensional changes, and homogenization. Therefore, the development of sintering additives in ceramic materials is frequently studied to improve operational flexibility and reduce sintering temperatures. The densification of ceramic samples at low sintering temperatures can be attributed to the appearance of low-melting phases and the formation of high concentrations of various defects. This phenomenon increases ion diffusion in the solid–liquid heterophase system and improves mass transfer and densification of the ceramic and grain growth. Overall, adding a sintering additive is a practical method for lowering the sintering temperature of ceramic materials to overcome the previously mentioned issues.

In recent years, researchers have investigated various types of metal oxides that can be used as additives to improve the sinterability of protonic electrolytes. A small number of metal oxides (MO_x)—where M is Ca, Ni, Cu, or Zn—can be used to lower the sintering temperature while maintaining acceptable electrochemical performance. Tong et al. [100] synthesized $BaZr_{0.8}Y_{0.2}O_3$ (BZY)with various metal sintering additives, including LiF, NiO, Al_2O_3, and SnO_2. They discovered a phase separation in the X-ray diffraction peaks of the BZY electrolyte with LiF and SnO_2 and a minor second cubic perovskite phase for Al_2O_3. In contrast, a single-phase cubic was observed by using 2 wt% NiO at 1400 °C. According to the literature [101–106], most previous studies used NiO, CuO, and ZnO as sintering additives due to their efficiency in increasing electrolyte densification at low sintering temperatures; most of these studies reported a decrease between 150 °C and 200 °C when a certain amount of the metal oxide is used.

Baral et al. [105] reported one of the lowest sintering temperatures for a Zr-containing electrolyte (1100 °C). This successful improvement has reduced sintering temperature and time from 1600 °C (20 h) to 1100 °C (5 h); this was achieved by adding 2 wt% ZnO into $BaCe_{0.35}Zr_{0.5}Y_{0.15}O_{2.95}$. However, the addition of ZnO has been associated with a decrease in protonic conductivity of the electrolytes [107]. Liu et al. [108] added 1 wt% NiO into the BZCYYb electrolyte. The modified BZCYYb–NiO showed excellent density and conductivity as compared to the pristine sample. The OCV gained was 1.088 V at 650 °C, which was satisfactory for fuel cell systems. Gao et al. [109] improved the densification properties of the $BaZr_{0.9}Y_{0.1}O_{3-\delta}$ electrolyte by applying 2 mol% CuO and sintering at 1600 °C for 4 h. The sample achieved 95.4% relative density, but a decrease in the conductivity by one magnitude was reported. Metal oxides, such as $LiNO_3$ [110], CaO, and Al_3O_2, have also been used, although they are not used widely due to their minor advantages in sample microstructure and electrochemical performance. Table 3 shows the various metal oxides used as sintering additives in the literature. Studies indicated that NiO and ZnO are suitable as sintering aids and help provide high OCV and power density values at temperatures < 600 °C.

Two methods are used for adding sintering additives—external and internal addition/doping—and they result in different electrolyte performances. Wang et al. [103] provided information about the use of different routes for adding 4 mol% NiO via internal doping and external addition to produce $BaZr_{0.1}Ce_{0.66}Ni_{0.04}Y_{0.2}O_{3-\delta}$ and $BaZr_{0.1}Ce_{0.7}Y_{0.2}O_{3-\delta}$–NiO, respectively. Both methods showed improved densification and electrical conductivity compared to the pristine BCZY sample at 1400 °C. The internally added NiO sample is fully dense with large grain sizes on average. In contrast, the externally added NiO sample produced smaller grain sizes with minimal pores. A similar study was conducted by Park et al. [104] to examine the effect of internally and externally added sintering additives to the $BaZr_{0.85}Yb_{0.15}O_{3-\delta}$ electrolyte. The samples were doped with 4% mol ZnO and sintered at 1400 °C for 10 h. Both samples presented a pure phase of BCZYb composition and demonstrated high relative density. The internally doped ZnO sample has a larger average grain size (1 μm) and obtained higher conductivity than the externally doped ZnO electrolyte (0.3 μm). This discrepancy was due to the minimal grain boundary, which exhibited a more significant ionic transportation while reducing grain boundary resistance than the submicron grains. A similar conclusion was reached by Baral et al. [105] who highlighted the existence of octahedral ZnO_6, in which Zn^{2+} operates as a dopant, which seemed beneficial for proton trapping in ZnO-added BCZY.

3.6. The conundrum of sintering aid

An important issue associated with the addition of sintering additives is the optimum amount of metal oxide used in electrolytes. Although using sintering additives provides solutions to high sintering temperature and related problems, the amount of metal oxide added should be carefully considered. An optimum amount of metal oxide exists; beyond this amount, its use negatively affects the sample performance. However, this optimum amount remains unclear. A high concentration of sintering additive may trigger additive aggregation in the sample powder, as stated by Lee et al. [106]. They were unsuccessful in analyzing the I–V performance after addition of a massive amount of 10 wt% NiO into the $BaCe_{0.6}Zr_{0.2}Y_{0.2}O_{3-\delta}$ electrolyte. This phenomenon suggested that the formation of NiO aggregation in the sample builds up the electronic transport between electrodes, and electrode crosstalk and decrease cell performance. Therefore, the optimum concentration to be added to the electrolyte is between 1 and 2 wt% NiO; this amount optimizes cell performance, especially in terms of electrical conductivity. Okuyama revealed that introducing > 5 wt% NiO decreased the electrical conductivity of the $BaCe_{0.6}Zr_{0.2}Y_{0.2}O_{3-\delta}$ electrolyte by about 3.5 times as compared to a pristine sample [102].

However, recent work by Han et al. [111] on the detrimental effect of using NiO as a sintering additive has revealed a decrease in proton concentration, which is vital for ionic conductivity and transport number, at any composition of the $BaZr_{1-x}Ce_xO_3$ electrolyte. NiO stimulates the proton trap in the electrolyte, which is caused by the electrostatic attraction between a negatively charged rare-earth component and a positively charged proton. The association of oxygen vacancies by the sintering additive is combined with the dopant additive ions, producing a cluster that can be influenced to trap migrating protons. Therefore, we believe an optimal amount of < 2 wt% NiO should be used as a sintering additive when using a single-doped $Ba(Ce,Zr)O_3$-based electrolyte (such as BCZY) to promote electrolyte densification while minimizing the effect of NiO on the ionic performance. In another study, Shimada reported that adding 2 wt% NiO to the BZCYYb electrolyte reduced the cell performance in terms of the power density but improved sinterability and thermal expansion behavior. The cell's OCV was 0.89 V, which is lower than that of a pristine cell (1.10 V), owing to the excessive NiO in the electrolyte, thereby resulting in a decrease in proton transportation.

4. Summary and future prospect

Thin-film structures improve the overall cell performance of electrolytes, such as the conductivity, cycling stability, and power density. Hence, the critical stage of developing dense electrolyte thin

Table 3
Comparison of cell performance with different sintering additives.

Electrolyte			Anode	Cathode	Sintering condition		Impurity element	D (μm)	Cell performance		Ref.
Nominal composition	Metal oxide	h (μm)			T (°C)	t (h)			OCV (V)	Power density ($mWcm^{-2}$)	
$BaZr_{0.8}Y_{0.2}O_{3-\delta}$	1 wt% NiO	25	$BaZr_{0.8}Y_{0.2}O_{3-\delta}$ + 60 wt% NiO	$BaCo_{0.4}Fe_{0.4}Zr_{0.1}Y_{0.1}O_{3-\delta}$	1450	18	None	N/A	1.02(600 °C)	660[1]	[112]
$BaCe_{0.7}Zr_{0.1}Y_{0.2}O_{3-\delta}$	2 mol% $Ni_{0.5}Fe_{0.5}$	20	$Ba_{0.96}(Ce_{0.66}Zr_{0.1}Ni_{0.04}Y_{0.2})O_{3-\delta}$	$La_{0.6}Sr_{0.4}Co_{0.2}Fe_{0.8}O_{3-\delta}$	1400	5	None	N/A	~1.0(700 °C)	10701	[113]
$BaCe_{0.7}Zr_{0.1}Y_{0.1}Yb_{0.1}O_{3-\delta}$	1 wt% NiO	~36	$BaCe_{0.7}Zr_{0.1}Y_{0.1}Yb_{0.1}O_{3-\delta}$ + 60 wt% NiO	$BaCo_{0.4}Fe_{0.4}Zr_{0.1}Y_{0.1}O_{3-\delta}$	Rapid laser reactive sintering method		None	2–5	0.94–0.97 (600 °C)	121[1]	[114]
$BaCe_{0.7}Zr_{0.1}Y_{0.2}O_{3-\delta}$	0.5 wt% NiO	217	$BaCe_{0.7}Zr_{0.1}Y_{0.2}O_{3-\delta}$ + 65 wt% NiO	$BaCe_{0.7}Zr_{0.1}Y_{0.2}O_{3-\delta}$ + 70 wt% $La_{0.6}Sr_{0.4}Co_{0.2}Fe_{0.8}O_{3-\delta}$	1400	6	BaY_2NiO_5	3.6	1.11(600 °C)	60[1]	[101]
$BaCe_{0.6}Zr_{0.2}Y_{0.2}O_{3-\delta}$	3 wt% NiO	~7	$BaCe_{0.6}Zr_{0.2}Y_{0.2}O_{3-\delta}$ + 65 wt% NiO	$La_{0.8}Sr_{0.2}Co_{0.8}Fe_{0.2}O_{3-\delta}$	1500	10	None	3–5	1.09(800 °C)	106.6[1]	[106]
$BaZr_{0.1}Ce_{0.66}Ni_{0.04}Y_{0.2}O_{3-\delta}$	NiO	12	$BaZr_{0.1}Ce_{0.66}Ni_{0.04}Y_{0.2}O_{3-\delta}$ + 60 wt% NiO	$BaZr_{0.1}Ce_{0.7}Y_{0.2}O_{3-\delta}$ + 50 wt% $Sm_{0.5}Sr_{0.5}CoO_{3-\delta}$	1400	5	None	N/A	1.053(600 °C)	477[1]	[103]
$BaZr_{0.6}Ce_{0.2}Y_{0.2}O_{3-\delta}$	3.56 wt% $Zn(NO_3)_2$	30	$BaZr_{0.6}Ce_{0.2}Y_{0.2}O_{3-\delta}$ + 60 wt% NiO	$BaZr_{0.6}Ce_{0.2}Y_{0.2}O_{3-\delta}$ + 70 wt% $La_{0.6}Sr_{0.4}Co_{0.2}Fe_{0.8}O_{3-\delta}$	1400	12	BaY_2NiO_5	4–6	1.08(600 °C)	336[2]	[49]
$BaZr_{0.80}Y_{0.16}Zn_{0.04}O_{3-\delta}$	1 wt% ZnO	~20	$BaZr_{0.8}Y_{0.2}O_{3-\delta}$ + 60 wt% NiO	Platinum	1450	5	BaY_2NiO_5	1–2	0.94(600 °C)	75[1]	[107]
$BaCe_{0.6}xZr_{0.2}Y_{0.15}Sm_{0.05}O_{3-\delta}$	4 wt% ZnO	39	$BaCe_{0.6}xZr_{0.2}Y_{0.15}Sm_{0.05}O_{3-\delta}$ + 50 wt% NiO	$(La_{0.75}Sr_{0.25})_{0.97}Cr_{0.5}Mn_{0.5}O_{3\pm\delta}$	1400	10	None	> 8	1.01(700 °C)	420[2]	[53]
$BaCe_{0.6}Zr_{0.3}Y_{0.1}O_{3-\delta}$	5 mol% CuO	~40	$BaCe_{0.6}Zr_{0.3}Y_{0.1}O_{3-\delta}$ + 60 wt% NiO	$BaCo_{0.4}Fe_{0.4}Zr_{0.1}Y_{0.1}O_{3-\delta}$	1450	N/A	None	~6.2	1.0–1.1(700 °C)	~550[2]	[115]
$BaCe_{0.5}Zr_{0.3}Dy_{0.2}O_{3-\delta}$	0.5 wt% CuO	30	$BaCe_{0.5}Zr_{0.3}Dy_{0.2}O_{3-\delta}$ + 60 wt% NiO	$Pr_{1.9}Ba_{0.1}NiO_{4+\delta}$	1350	5	N/A	N/A	0.935(700 °C)	470[1]	[64]
$BaZr_{0.8}Y_{0.2}O_{3-\delta}$	4 mol% CaO	25	$BaZr_{0.8}Y_{0.2}O_{3-\delta}$ + 60 wt% NiO	$BaZr_{0.8}Y_{0.2}O_{3-\delta}$ + 60 vol% $La_{0.6}Sr_{0.4}Co_{0.2}Fe_{0.8}O_{3-\delta}$	1500	6	None	0.36	0.99(700 °C)	141[1]	[60]
$BaZr_{0.8}Y_{0.2}O_{3-\delta}$	$LiNO_3$	25	$BaZr_{0.8}Y_{0.2}O_{3-\delta}$ + 60 wt% NiO	$BaZr_{0.8}Y_{0.2}O_{3-\delta}$ + 60 vol% $La_{0.6}Sr_{0.4}Co_{0.2}Fe_{0.8}O_{3-\delta}$	1450	5	None	0.4–1.0	0.98(700 °C)	53[1]	[110]

Abbreviations: temperature (T), time (t), electrolyte thickness (h), (TC), average grain size (D). [1]Cell condition in humidified H_2 and air. [2]Cell condition in humidified H_2/Ar and air.

films needs to be deeply investigated. The best-suited fabrication process for the materials used as SOFC components must be carefully determined. Furthermore, material selection, the purpose of research, and a cost-effective fabrication procedure must be considered when developing a simple design for PCFC applications. The use of nanoparticles or nanograins provides a novel opportunity to investigate the benefits of nanomaterials in PCFCs. The effects of particle size on electrolyte performance have established that the optimal grain size is 50–100 nm. Smaller grains introduce contaminants that impair cell performance. A substantial change in ionic conductivity and power density can be expected from using nanoscale materials during cell operation, which is selective to operating temperatures.

We have highlighted appropriate fabrication techniques for developing electrolyte films for PCFCs. Conventional methods are the most cost-effective and efficient ones, but they require batch processing and are time consuming. In comparison, unconventional sintering methods, particularly SPS, can be viable for fabricating multicomponent composites and are promising for experimental purposes, despite their high maintenance costs. SPS, which is a vital tool for preparing advanced materials, particularly nanostructured ones such as ceramics, has become progressively essential to fabricating high-quality electrolyte thin films for PCFC applications and is a way to solve a wide range of technological problems.

Electrolyte thermal treatment is critical to the microstructure of the thin layer. Conventional sintering methods are simple but require higher temperatures and longer time to sinter. Unconventional methods rely on the addition of pressure to conduct at lower temperatures and at a quicker rate than conventional methods and are also suitable to produce fine particles, as these approaches may inhibit grain growth.

5. Conclusion

Anode-supported PCFCs with thin-film electrolytes contribute significantly to the lowering of operational temperatures. They provide excellent electrochemical properties and are reliant on the SOFC's thin-film structure. To ensure an optimal ionic path in the electrolyte during gas transfer, we considered all aspects of the fabrication process, such as materials, conditions, and parameters. Using nanomaterials enables the formation of a dense electrolyte thin film while improving its electrochemical properties at low operating temperatures. In terms of fabrication methods, screen printing and tape casting are the most appropriate methods for the mass production of electrolyte thin films because of their simplicity and ability to produce credible electrolyte films comparable to those produced by other sophisticated procedures. Even if a sophisticated route is required, these methods are preferable because they can produce an extremely thin electrolyte film, thereby reducing ohmic resistance and enabling ionic mobilization to occur within a much shorter length.

Declaration of Competing Interest

The authors declare that they have no known competing financial interests or personal relationships that could have appeared to influence the work reported in this paper.

Acknowledgments

This study is financially supported by Universiti Teknologi MARA-Universiti Teknologi Malaysia (100-RMC 5/3/SRP GOV (0022021)); and Universiti Teknologi MARA (100-TNCPI/INT 16/6/2 (033/2021))-National Central University (CER-110IN0601) for the Matching Research Grant 2021.

References

[1] I. Staffell, D. Scamman, V. Abad, P. Balcombe, P.E. Dodds, P. Ekins, K.R. Ward, A. Velazquez Abad, P. Balcombe, P.E. Dodds, P. Ekins, N. Shah, K.R. Ward, The role of hydrogen and fuel cells in the global energy system, Energy Environ. Sci. 12 (2018) 463–491, https://doi.org/10.1039/c8ee01157e

[2] R. Fernández-González, E. Hernández, S. Savvin, P. Núñez, A. Makradi, N. Sabaté, J.J.P. Esquivel, J.C.J.C. Ruiz-Morales, R. Fernandez-Gonzalez, E. Hernandez, S. Savvin, P. Nunez, A. Makradi, N. Sabate, J.J.P. Esquivel, J.C.J.C. Ruiz-Morales, A novel microstructured metal-supported solid oxide fuel cell, J. Power Sources 272 (2014) 233–238, https://doi.org/10.1016/j.jpowsour.2014.08.081

[3] R. Hui, Z. Wang, O. Kesler, L. Rose, J. Jankovic, S. Yick, R. Maric, D. Ghosh, Thermal plasma spraying for SOFCs: applications, potential advantages, and challenges, J. Power Sources 170 (2007) 308–323, https://doi.org/10.1016/j.jpowsour.2007.03.075

[4] P. Coddet, H.L. Christian, C. Coddet, A review on high power SOFC electrolyte layer manufacturing using thermal spray and physical vapour deposition technologies, Adv. Manuf. (2013), https://doi.org/10.1007/s40436-013-0049-7

[5] X. Xu, C. Xia, S. Huang, D. Peng, YSZ thin films deposited by spin-coating for IT-SOFCs, Ceram. Int. 31 (2005) 1061–1064, https://doi.org/10.1016/j.ceramint.2004.11.005

[6] H. Il Ji, J.H. Lee, J.W. Son, K.J. Yoon, S. Yang, B.K. Kim, Protonic ceramic electrolysis cells for fuel production: a brief review, J. Korean Ceram. Soc. 57 (2020) 480–494, https://doi.org/10.1007/s43207-020-00059-4

[7] E.C.C. De Souza, R. Muccillo, Properties and applications of perovskite proton conductors, Mater. Res. 13 (2010) 385–394, https://doi.org/10.1590/s1516-14392010000300018

[8] E. Fabbri, D. Pergolesi, E. Traversa, Materials challenges toward proton-conducting oxide fuel cells: a critical review, Chem. Soc. Rev. 39 (2010) 4355–4369, https://doi.org/10.1039/b902343g

[9] S. Hossain, A.M. Abdalla, S.N.B. Jamain, J.H. Zaini, A.K. Azad, S. Noorazean, B. Jamain, J.H. Zaini, A.K. Azad, S.N.B. Jamain, J.H. Zaini, A.K. Azad, S. Noorazean, S.N.B. Jamain, J. Hj Zaini, A.K. Azad, A review on proton conducting electrolytes for clean energy and intermediate temperature-solid oxide fuel cells, Renew. Sustain. Energy Rev. 79 (2017) 750–764, https://doi.org/10.1016/j.rser.2017.05.147

[10] A. Uthayakumar, M. Kavithanjali, K. Sandhya, N. Ponpandian, K.S. Babu, The rare earth dopant (La, Gd, Sm & Y) modulated grain boundary energy barrier suppression in BaZrO3-BaCeO3 solid solution, J. Alloy. Compd. 864 (2021), https://doi.org/10.1016/j.jallcom.2020.158098

[11] N. Nasani, Z. Shakel, F.J.A. Loureiro, B.B. Panigrahi, B.B. Kale, D.P. Fagg, Exploring the impact of sintering additives on the densification and conductivity of BaCe0.3Zr0.55Y0.15O3-δ electrolyte for protonic ceramic fuel cells, J. Alloy. Compd. 862 (2021) 158640, https://doi.org/10.1016/j.jallcom.2021.158640

[12] F.C. Antunes, C.A. Goulart, M.R.B. Andreeta, D.P.F. de Souza, YSZ/Al2O3 multilayer thick films deposited by spin coating using ceramic suspensions on Al2O3 polycrystalline substrate, Mater. Sci. Eng. B Solid-State Mater. Adv. Technol. 228 (2018) 60–66, https://doi.org/10.1016/j.mseb.2017.11.007

[13] K. Katahira, Y. Kohchi, T. Shimura, H. Iwahara, Protonic conduction in Zr-substituted BaCeO3, Solid State Ion. 138 (2000) 91–98, https://doi.org/10.1016/S0167-2738(00)00777-3

[14] T. Takahashi, H. Iwahara, Ionic conduction in perovskite-type oxide solid solution and its application to the solid electrolyte fuel cell, Energy Convers. 11 (1971) 105–111, https://doi.org/10.1016/0013-7480(71)90121-5

[15] H. Iwahara, H. Uchida, S. Tanaka, High temperature type proton conductor based on SrCeO3 and its application to solid electrolyte fuel cells, Solid State Ion. 9–10 (1983) 1021–1025, https://doi.org/10.1016/0167-2738(83)90125-X

[16] H. Iwahara, H. Uchida, K. Ono, K. Ogaki, Proton conduction in sintered oxides based on BaCeO3, J. Electrochem. Soc. 135 (1988) 529–533, https://doi.org/10.1149/1.2095649

[17] S. Wienströer, H.D. Wiemhöfer, Investigation of the influence of zirconium substitution on the properties of neodymium-doped barium cerates, Solid State Ion. 101–103 (1997) 1113–1117, https://doi.org/10.1016/s0167-2738(97)00163-x

[18] C.J. Tseng, J.K. Chang, K.R. Lee, I.M. Hung, J.C. Lin, S.C. Jang, S.W. Lee, Potassium doping optimization in proton-conducting Ba1-xKxCe0.6Zr0.2Y0.2O3-δ oxides for fuel cell applications, J. Alloy. Compd. 696 (2017) 251–256, https://doi.org/10.1016/j.jallcom.2016.11.249

[19] C. Zhou, J. Sunarso, Y. Song, J. Dai, J. Zhang, B. Gu, W. Zhou, Z. Shao, New reduced-temperature ceramic fuel cells with dual-ion conducting electrolyte and triple-conducting double perovskite cathode, J. Mater. Chem. A 7 (2019) 13265–13274, https://doi.org/10.1039/c9ta03501j

[20] S. Rajendran, N.K. Thangavel, S. Alkatie, Y. Ding, L.M.R. Arava, Y, Gd, and Pr tri-doped perovskite-type proton conducting electrolytes with improved sinterability and chemical stability, J. Alloy. Compd. 870 (2021) 1–24, https://doi.org/10.1016/j.jallcom.2021.159431

[21] B. Mirfakhraei, F. Ramezanipour, S. Paulson, V. Birss, V. Thangadurai, Effect of sintering temperature on microstructure, chemical stability, and electrical properties of transition metal or Yb-doped BaZr 0.1 Ce 0.7 Y 0.1 M 0.1 O 3-δ (M = Fe, Ni, Co, and Yb), Front. Energy Res. 2 (2014) 1–10, https://doi.org/10.3389/fenrg.2014.00009

[22] J. Sui, L. Cao, Q. Zhu, L. Yu, Q. Zhang, L. Dong, Effects of proton-conducting electrolyte microstructure on the performance of electrolyte-supported solid oxide fuel cells, J. Renew. Sustain. Energy 5 (2013), https://doi.org/10.1063/1.4798491

[23] F.J.A. Loureiro, N. Nasani, G.S. Reddy, N.R. Munirathnam, D.P. Fagg, A review on sintering technology of proton conducting BaCeO3 -BaZrO3 perovskite oxide materials for protonic ceramic fuel cells, J. Power Sources 438 (2019).

[24] J. Tong, M. Shang, R. Patrick O'Hayre, S. Menzer, W.G. Coors, Cost-Effective Solid State Reactive Sintering Method for Protonic Ceramic Fuel Cells, 10305116, 2019.

[25] Y. Li, J. Zhao, B. Wang, Low temperature preparation of nanocrystalline Sr0.5Ba0.5Nb2O6 powders using an aqueous organic gel route, Mater. Res. Bull. 39 (2004) 365–374, https://doi.org/10.1016/j.materresbull.2003.11.002

[26] N.A. Abdullah, A. Sharizal, N. Osman, Role of CA-EDTA on the synthesizing process of cerate-zirconate ceramics electrolyte, J. Chem. (2013) (2013).

[27] G. Chiodelli, L. Malavasi, C. Tealdi, S. Barison, M. Battagliarin, L. Doubova, M. Fabrizio, C. Mortalò, R. Gerbasi, Role of synthetic route on the transport properties of BaCe1-xYxO3 proton conductor, J. Alloy. Compd. 470 (2009) 477–485, https://doi.org/10.1016/j.jallcom.2008.03.011

[28] K. Lee, J. Lee, H. Yoo, Grain size effect on the electrical properties of nanocrystalline ceria, J. Eur. Ceram. Soc. 34 (2014) 2363–2370, https://doi.org/10.1016/j.jeurceramsoc.2014.02.035

[29] G. Chen, X. Zhang, Y. Luo, Y. He, H. Liu, S. Geng, K. Yu, Y. Dong, Ionic conduction mechanism of a nanostructured BCY electrolyte for low-temperature SOFC, Int. J. Hydrog. Energy 45 (2020) 24108–24115, https://doi.org/10.1016/j.ijhydene.2019.07.223

[30] N. Asyikin, N. Syafkeena, A. Mohd, N. Waheeda, A. Mutalib, Optimization of electrolyte performance by tailoring the structure and morphology of Ba(Ce,Zr)O3 ceramics with different types of surfactants, Ceram. Int. 46 (2020) 27401–27409, https://doi.org/10.1016/j.ceramint.2020.07.226

[31] S. Wang, L.L. Zhang, L.L. Zhang, K. Brinkman, F. Chen, Two-step sintering of ultrafine-grained barium cerate proton conducting ceramics, Electrochim. Acta 87 (2013) 194–200, https://doi.org/10.1016/j.electacta.2012.09.007

[32] S.H. Min, J.G. Lee, O.S. Jeon, M.G. Park, K.H. Ryu, J. ha Myung, Y.G. Shul, Characteristics of Ba(Zr0.1Ce0.7Y0.2)O3-δ nano-powders synthesized by different wet-chemical methods for solid oxide fuel cells, Ceram. Int. 44 (2018) 433–437, https://doi.org/10.1016/j.ceramint.2017.09.195

[33] X. Ma, J. Dai, H. Zhang, D.E. Reisner, Protonic conductivity nanostructured ceramic film with improved resistance to carbon dioxide at elevated temperatures, Surf. Coat. Technol. 200 (2005) 1252–1258, https://doi.org/10.1016/j.surfcoat.2005.07.099

[34] H.J. Park, J.W. Roh, Protonic conduction of nanostructured Y-doped BaZrO3, J. Nanomater. 2016 (2016) 1–7, https://doi.org/10.1155/2016/8757305

[35] R.B. Cervera, Y. Oyama, S. Miyoshi, I. Oikawa, H. Takamura, S. Yamaguchi, Nanograined Sc-doped BaZrO 3 as a proton conducting solid electrolyte for intermediate temperature solid oxide fuel cells (IT-SOFCs), Solid State Ion. 264 (2014) 1–6, https://doi.org/10.1016/j.ssi.2014.06.010

[36] M.G. Bellino, D.G. Lamas, N.E.W.De Reca, Enhanced ionic conductivity in nanostructured, heavily doped ceria ceramics, Adv. Funct. Mater. 16 (2006) 107–113, https://doi.org/10.1002/adfm.200500186

[37] J.M. Park, D.Y. Kim, J.D. Baek, Y.J. Yoon, P.C. Su, S.H. Lee, Effect of electrolyte thickness on electrochemical reactions and thermo-fluidic characteristics inside a SOFC unit cell, Energies 11 (2018), https://doi.org/10.3390/en11030473

[38] R. Balzarotti, C. Cristiani, L.F. Francis, Combined dip-coating/spin-coating depositions on ceramic honeycomb monoliths for structured catalysts preparation, Catal. Today 334 (2019) 90–95, https://doi.org/10.1016/j.cattod.2019.01.037

[39] T. Vijay Kumar, G. Kumar, R. Venkateswarlu, A. Sadananada Chary, S. Narender Reddy, Preparation of nano-sized particles of Sr(NO3)2 solid electrolyte by planetary ball milling, Mater. Today Proc. 5 (2018) 26894–26897, https://doi.org/10.1016/j.matpr.2018.08.174

[40] A.R. Hanifi, N.K. Sandhu, T.H. Etsell, J.L. Luo, P. Sarkar, Fabrication and characterization of a tubular ceramic fuel cell based on BaZr0.1Ce0.7Y0.1Yb0.1O3-δ proton conducting electrolyte, J. Power Sources 341 (2017) 264–269, https://doi.org/10.1016/j.jpowsour.2016.12.010

[41] D. Cao, M. Zhou, X. Yan, Z. Liu, J. Liu, High performance low-temperature tubular protonic ceramic fuel cells based on barium cerate-zirconate electrolyte, Electrochem. Commun. 125 (2021) 106986, https://doi.org/10.1016/j.elecom.2021.106986

[42] J. Xiao, W. Sun, Z. Zhu, Z. Tao, W. Liu, Fabrication and characterization of anode-supported dense BaZr 0.8Y 0.2O 3-δ electrolyte membranes by a dip-coating process, Mater. Lett. 73 (2012) 198–201, https://doi.org/10.1016/j.matlet.2012.01.032

[43] R. Ren, Z. Wang, C. Xu, W. Sun, J. Qiao, D.W. Rooney, K. Sun, Tuning the defects of the triple conducting oxide BaCo0.4Fe0.4Zr0.1Y0.1O3-: δ perovskite toward enhanced cathode activity of protonic ceramic fuel cells, J. Mater. Chem. A 7 (2019) 18365–18372, https://doi.org/10.1039/c9ta04335g

[44] C. Geng, X. Yu, P. Wang, J. Cheng, T. Hong, The rapid one-step fabrication of bilayer anode for protonic ceramic fuel cells by phase inversion tape casting, J. Eur. Ceram. Soc. 40 (2020) 3104–3110, https://doi.org/10.1016/j.jeurceramsoc.2020.02.020

[45] L. Lei, Y. Bai, Y. Liu, An investigation on dip-coating technique for fabricating anode-supported solid oxide fuel cells, Int. J. Appl. Ceram. Technol. 7 (2013) 1–7, https://doi.org/10.1111/ijac.12147

[46] R.J. Yang, M.C. Lee, J.C. Chang, T.N. Lin, Y.C. Chang, W.X. Kao, L.S. Lee, S.W. Cheng, Fabrication and characterization of a Sm 0.2Ce 0.8O 1.9 electrolyte film by the spin-coating method for a low-temperature anode-supported solid oxide fuel cells, J. Power Sources 206 (2012) 111–118, https://doi.org/10.1016/j.jpowsour.2012.01.024

[47] H. Shimada, Y. Yamaguchi, H. Sumi, Y. Mizutani, Enhanced La0.6Sr0.4Co0.2Fe0.8O3–δ-based cathode performance by modification of BaZr0.1Ce0.7Y0.1Yb0.1O3–δ electrolyte surface in protonic ceramic fuel cells, Ceram. Int. 47 (2021) 16358–16362, https://doi.org/10.1016/j.ceramint.2021.02.123

[48] N. Nasani, D. Ramasamy, S. Mikhalev, A.V.V. Kovalevsky, D.P.P. Fagg, Fabrication and electrochemical performance of a stable, anode supported thin BaCe0.4Zr0.4Y0.2O3-δ electrolyte protonic ceramic fuel cell, J. Power Sources 278 (2015) 582–589, https://doi.org/10.1016/j.jpowsour.2014.12.124

[49] S. Jeong, T. Kobayashi, K. Kuroda, H. Kwon, C. Zhu, H. Habazaki, Y. Aoki, Evaluation of thin film fuel cells with Zr-rich BaZr: XCe0.8- xY0.2O3- δ electrolytes (x ≥ 0.4) fabricated by a single-step reactive sintering method, RSC Adv. 8 (2018) 26309–26317, https://doi.org/10.1039/c8ra04724c

[50] H. Shimada, T. Yamaguchi, H. Sumi, Y. Yamaguchi, K. Nomura, Additive effect of NiO on electrochemical properties of mixed ion conductor BaZr0.1Ce0.7Y0.1Yb0.1O3-δ, J. Ceram. Soc. Jpn. 125 (2017) 257–261, https://doi.org/10.2109/jcersj2.16237

[51] E.H. Kang, H.R. Choi, J.S. Parl, K.H. Kim, D.H. Kim, K. Bae, F.B. Prinz, J.H. Shim, Protonic ceramic fuel cells with slurry-spin coated BaZr0.2Ce0.6Y0.1Yb0.1O3-δ thin-film electrolytes, J. Power Sources 465 (2020) 1–8.

[52] N.A. Baharuddin, N.F. Abdul Rahman, H. Abd. Rahman, M.R. Somalu, M.A. Azmi, J. Raharjo, Fabrication of high-quality electrode films for solid oxide fuel cell by screen printing: a review on important processing parameters, Int. J. Energy Res. 44 (2020) 8296–8313, https://doi.org/10.1002/er.5518

[53] S. Hossain, A.M. Abdalla, J.H. Zaini, C.D. Savaniu, J.T.S. Irvine, A.K. Azad, Highly dense and novel proton conducting materials for SOFC electrolyte, Int. J. Hydrog. Energy 42 (2017) 27308–27322, https://doi.org/10.1016/j.ijhydene.2017.09.067

[54] S.M. Choi, J.H.H. Lee, H. Il Ji, K.J. Yoon, J.W. Son, B.K. Kim, H.J. Je, H.W. Lee, Fabrication and characterization of Ba(Zr0.84Y 0.15Cu0.01)O3-δ electrolyte-based protonic ceramic fuel cells, Ceram. Int. 39 (2013) 9605–9611, https://doi.org/10.1016/j.ceramint.2013.05.081

[55] Y. Meng, J. Duffy, B.T. Na, J. Gao, T. Yang, J. Tong, S. Lee, K.S. Brinkman, Oxygen exchange and bulk diffusivity of BaCo0.4Fe0.4Zr0.1Y0.1O3-δ: quantitative assessment of active cathode material for protonic ceramic fuel cells, Solid State Ion. 368 (2021) 115639, https://doi.org/10.1016/j.ssi.2021.115639

[56] K. Bae, H.S. Noh, D.Y. Jang, J. Hong, H. Kim, K.J. Yoon, J.H. Lee, B.K. Kim, J.H. Shim, J.W. Son, High-performance thin-film protonic ceramic fuel cells fabricated on anode supports with a non-proton-conducting ceramic matrix, J. Mater. Chem. A 4 (2016) 6395–6404, https://doi.org/10.1039/c5ta10670b

[57] D. Konwar, H.H. Yoon, A methane-fueled SOFC based on a thin BaZr0.1Ce0.7Y0.1Yb0.1O3-δ electrolyte film and a LaNi0.6Co0.4O3 anode functional layer, J. Mater. Chem. A 4 (2016) 5102–5106, https://doi.org/10.1039/c5ta10689c

[58] S. Lobe, A. Bauer, S. Uhlenbruck, D. Fattakhova-Rohlfing, Physical vapor deposition in solid-state battery development: from materials to devices, Adv. Sci. 8 (2021) 1–33, https://doi.org/10.1002/advs.202002044

[59] L. Bi, E. Fabbri, E. Traversa, Effect of anode functional layer on the performance of proton-conducting solid oxide fuel cells (SOFCs), Electrochem. Commun. 16 (2012) 37–40, https://doi.org/10.1016/j.elecom.2011.12.023

[60] Z. Sun, E. Fabbri, L. Bi, E. Traversa, Electrochemical properties and intermediate-temperature fuel cell performance of dense yttrium-doped barium zirconate with calcium addition, J. Am. Ceram. Soc. 95 (2012) 627–635, https://doi.org/10.1111/j.1551-2916.2011.04795.x

[61] L. Li, Q. Zhong, Y. Bu, Y. Song, Improvement of BaCe0.8Sm0.1Y0.1O3-δ-based IT-SOFC by optimizing spin-coated process of cathode and sintering temperature, Ionics 21 (2015) 817–822, https://doi.org/10.1007/s11581-014-1219-8

[62] S. Wu, X. Xu, X. Li, L. Bi, High-performance proton-conducting solid oxide fuel cells using the first-generation Sr-doped LaMnO3 cathode tailored with Zn ions, Sci. China Mater. (2021) 1–8.

[63] J. Lyagaeva, G. Vdovin, L. Hakimova, D. Medvedev, A. Demin, P. Tsiakaras, BaCe0.5Zr0.3Y0.2–xYbxO3–d proton-conducting electrolytes for intermediate-temperature solid oxide fuel cells, Electrochim. Acta 251 (2017) 554–561, https://doi.org/10.1016/j.electacta.2017.08.149

[64] A. Tarutin, N. Danilov, J. Lyagaeva, D. Medvedev, One-step fabrication of protonic ceramic fuel cells using a convenient tape calendering method, Appl. Sci. 10 (2020).

[65] D. Medvedev, J. Lyagaeva, G. Vdovin, S. Beresnev, A. Demin, P. Tsiakaras, A tape calendering method as an effective way for the preparation of proton ceramic fuel cells with enhanced performance, Electrochim. Acta 210 (2016) 681–688, https://doi.org/10.1016/j.electacta.2016.05.197

[66] S. Lee, S. Park, S. Wee, D. Shin, One-dimensional structured La0.6Sr0.4Co0.2Fe0.8O3-δ - BaCe0.5Zr0.35Y0.15O3-δ composite cathode for protonic ceramic fuel cells, Solid State Ion. 320 (2018) 347–352, https://doi.org/10.1016/j.ssi.2018.03.010

[67] D. Konwar, B.J. Park, P. Basumatary, H.H. Yoon, Enhanced performance of solid oxide fuel cells using BaZr0.2Ce0.7Y0.1O3−Δ thin films, J. Power Sources 353 (2017) 254–259, https://doi.org/10.1016/j.jpowsour.2017.04.010

[68] G. Taillades, P. Pers, V. Mao, M. Taillades, High performance anode-supported proton ceramic fuel cell elaborated by wet powder spraying, Int. J. Hydrog. Energy 41 (2016) 12330–12336, https://doi.org/10.1016/j.ijhydene.2016.05.094

[69] M.P. Carpanese, A. Barbucci, G. Canu, M. Viviani, BaCe0.85Y0.15O2.925 dense layer by wet powder spraying as electrolyte for SOFC/SOEC applications, Solid State Ion. 269 (2015) 80–85, https://doi.org/10.1016/j.ssi.2014.11.014

[70] Y. Yoo, N. Lim, Performance and stability of proton conducting solid oxide fuel cells based on yttrium-doped barium cerate-zirconate thin-film electrolyte, J. Power Sources 229 (2013) 48–57, https://doi.org/10.1016/j.jpowsour.2012.11.094

[71] J. Xiao, L. Chen, H. Yuan, L. Ji, C. Xiong, J. Ma, X. Zhu, Fabrication and characterization of BaZr0.1Ce0.7Y0.2O3−δ based anode supported solid oxide fuel cells by tape casting combined with spray coating, Mater. Lett. 189 (2017) 192–195, https://doi.org/10.1016/j.matlet.2016.10.114

[72] J. Bu, P.G. Jönsson, Z. Zhao, Ionic conductivity of dense BaZr0.5Ce0.3Ln0.2O3-δ (Ln = Y, Sm, Gd, Dy) electrolytes, J. Power Sources 272 (2014) 786–793, https://doi.org/10.1016/j.jpowsour.2014.09.056

[73] J. Bu, P.G. Jonsson, Z. Zhao, Transport properties of BaZr0.5Ce0.3Y0.2O3-δ proton conductor prepared by spark plasma sintering, Ceram. Int. (2015), https://doi.org/10.1016/j.ceramint.2015.11.121

[74] M.-Y. Chu, L.C. De Jonghe, M.K.F. Lin, Pre-coarsening to improve microstructure and sintering of power compacts, J. Am. Ceram. Soc. (1990) 35–43.

[75] J.L. Huang, L.M. Din, H.H. Lu, W.H. Chan, Effects of two-step sintering on the microstructure of Si3N4, Ceram. Int. 22 (1996) 131–136, https://doi.org/10.1016/0272-8842(95)00068-2

[76] I.W. Chen, X.H. Wang, Sintering dense nanocrystalline ceramics without final-stage grain growth, Nature 404 (2000) 168–171.

[77] H. Sun, X. Guo, J. Li, G. Li, Z. Yang, H. Ding, W. Yan, S. Qi, P. Wang, Y. Song, Effect of grain size on the electrical performance of BaZr0.1Ce0.7Y0.1Yb0.1O3-δ solid electrolytes with addition of NiO, Ceram. Int. 45 (2019) 622–626, https://doi.org/10.1016/j.ceramint.2018.09.217

[78] H. Ding, X. Xue, BaZr0.1Ce0.7Y0.1Yb0.1O3-δ electrolyte-based solid oxide fuel cells with cobalt-free PrBaFe2O5+δ layered perovskite cathode, J. Power Sources 195 (2010) 7038–7041, https://doi.org/10.1016/j.jpowsour.2010.05.010

[79] B. Lin, M. Hu, J. Ma, Y. Jiang, S. Tao, G. Meng, Stable, easily sintered BaCe0.5Zr0.3y 0.16Zn0.04O3-δ electrolyte-based protonic ceramic membrane fuel cells with Ba0.5Sr0.5Zn 0.2Fe0.8O3-δ perovskite cathode, J. Power Sources 183 (2008) 479–484, https://doi.org/10.1016/j.jpowsour.2008.05.075

[80] S. Wang, L. Zhang, Z. Yang, L. Zhang, S. Fang, K. Brinkman, F. Chen, Two-step co-sintering method to fabricate anode-supported Ba3Ca 1.18Nb1.82O 9-δ proton-conducting solid oxide fuel cells, J. Power Sources 215 (2012) 221–226, https://doi.org/10.1016/j.jpowsour.2012.05.009

[81] M. Suarez, A. Fernandez, J.L. Menendez, R. Torrecillas, H. U, J. Hennicke, R. Kirchner, T. Kessel, Challenges and opportunities for spark plasma sintering: a key technology for a new generation of materials, Sinter. Appl. (2013), https://doi.org/10.5772/53706

[82] S. Wang, Y. Liu, J. He, F. Chen, K.S. Brinkman, Spark-plasma-sintered barium zirconate based proton conductors for solid oxide fuel cell and hydrogen separation applications, Int. J. Hydrog. Energy 40 (2015) 5707–5714, https://doi.org/10.1016/j.ijhydene.2015.02.116

[83] T.L. Simonenko, M.V. Kalinina, N.P. Simonenko, E.P. Simonenko, O.V. Glumov, N.A. Mel, I.V. Murin, O.O. Shichalin, E.K. Papynov, O.A. Shilova, V.G. Sevastyanov, N.T. Kuznetsov, Synthesis of BaCe0.9-xZrxY0.1O3-d nanopowders and the study of proton conductors fabricated on their basis by low-temperature spark plasma sintering, Int. J. Hydrog. Energy 4 (2019), https://doi.org/10.1016/j.ijhydene.2019.05.231

[84] V.R. Mudinepalli, S. Song, J. Li, B.S. Murty, A comparative study of structural and electrical properties of Ba0.8Pb0.2TiO3 nanocrystalline ceramics prepared by microwave and spark plasma sintering, Mater. Chem. Phys. 142 (2013) 686–691, https://doi.org/10.1016/j.matchemphys.2013.08.023

[85] X. Xu, L. Bi, X.S. Zhao, Highly-conductive proton-conducting electrolyte membranes with a low sintering temperature for solid oxide fuel cells, J. Membr. Sci. 558 (2018) 17–25, https://doi.org/10.1016/j.memsci.2018.04.037

[86] B. Wang, L. Bi, X.S. Zhao, Fabrication of one-step co-fired proton-conducting solid oxide fuel cells with the assistance of microwave sintering, J. Eur. Ceram. Soc. 38 (2018) 5620–5624, https://doi.org/10.1016/j.jeurceramsoc.2018.08.020

[87] H. Dai, Proton conducting solid oxide fuel cells with chemically stable BaZr0.75Y0.2Pr0.05O3-δ electrolyte, Ceram. Int. 43 (2017) 7362–7365, https://doi.org/10.1016/j.ceramint.2017.02.090

[88] X. Meng, N. Yang, J. Song, X. Tan, Z.F. Ma, K. Li, Synthesis and characterization of terbium doped barium cerates as a proton conducting SOFC electrolyte, Int. J. Hydrog. Energy 36 (2011) 13067–13072, https://doi.org/10.1016/j.ijhydene.2011.07.075

[89] L. Bi, E. Fabbri, Z. Sun, E. Traversa, Sinteractive anodic powders improve densification and electrochemical properties of BaZr0.8Y0.2O3-δ electrolyte films for anode-supported solid oxide fuel cells, Energy Environ. Sci. 4 (2011) 1352–1357, https://doi.org/10.1039/c0ee00387e

[90] D. Han, L. Jiang, P. Zhong, Improving phase compatibility between doped BaZrO3 and NiO in protonic ceramic cells via tuning composition and dopant, Int. J. Hydrog. Energy 46 (2021) 8767–8777, https://doi.org/10.1016/j.ijhydene.2020.12.075

[91] Y. Guo, Y. Lin, R. Ran, Z. Shao, Zirconium doping effect on the performance of proton-conducting BaZryCe0.8−yY0.2O3−ı (0.0≤y≤0.8) for fuel cell applications, J. Power Sources 193 (2009) 400–407, https://doi.org/10.1016/j.jpowsour.2009.03.044

[92] F. Zhao, S. Wang, L. Dixon, F. Chen, Novel BaCe0.7In0.2Yb0.1O 3-δ proton conductor as electrolyte for intermediate temperature solid oxide fuel cells, J. Power Sources 196 (2011) 7500–7504, https://doi.org/10.1016/j.jpowsour.2011.04.036

[93] R. Haugsrud, T. Norby, Proton conduction in rare-earth ortho-niobates and ortho-tantalates, Nat. Mater. (2006), https://doi.org/10.1038/nmat1591

[94] N.Q. Minh, Solid oxide fuel cell technology - features and applications, Solid State Ion. 174 (2004) 271–277, https://doi.org/10.1016/j.ssi.2004.07.042

[95] M. Chen, M. Zhou, Z. Liu, J. Liu, A comparative investigation on protonic ceramic fuel cell electrolytes BaZr0.8Y0.2O3-δ and BaZr0.1Ce0.7Y0.2O3-δ with NiO as sintering aid, Ceram. Int. (2022), https://doi.org/10.1016/j.ceramint.2022.02.278

[96] M. Irshad, Q. ul Ain, K. Siraj, R. Raza, A.N. Tabish, M. Rafique, R. Idrees, F. Khan, S. Majeed, M. Ahsan, Evaluation of BaZr0.8X0.2 (X= Y, Gd, Sm) proton conducting electrolytes sintered at low temperature for IT-SOFC synthesized by cost effective combustion method, J. Alloy. Compd. 815 (2020), https://doi.org/10.1016/j.jallcom.2019.152389

[97] D. Han, K. Kishida, H. Inui, T. Uda, Substantial appearance of origin of conductivity decrease in Y-doped BaZrO3 due to Ba-deficiency, R. Soc. Chem. (2014) 31589–31593, https://doi.org/10.1039/C4RA04488F

[98] M. Nobre, R. Ananth, M. Nobre, What are Sintering Aids and How to Choose It?, 2015.

[99] N. Kumar, A. Singh, D.K. Sharma, K. Kishore, Toxicity of food additives, Food Saf. Hum. Health (2019), https://doi.org/10.1016/B978-0-12-816333-7.00003-5

[100] J. Tong, D. Clark, M. Hoban, R. O'Hayre, Cost-effective solid-state reactive sintering method for high conductivity proton conducting yttrium-doped barium zirconium ceramics, Solid State Ion. 181 (2010) 496–503, https://doi.org/10.1016/j.ssi.2010.02.008

[101] Z. Liu, X. Wang, M. Liu, J. Liu, Enhancing sinterability and electrochemical properties of Ba(Zr0.1Ce0.7Y0.2)O3-Δ proton conducting electrolyte for solid oxide fuel cells by addition of NiO, Int. J. Hydrog. Energy 43 (2018) 13501–13511, https://doi.org/10.1016/j.ijhydene.2018.05.089

[102] Y. Okuyama, N. Ebihara, K. Okuyama, Y. Mizutani, Improvement of protonic ceramic fuel cells with thin film BCZY electrolyte, ECS Trans. 68 (2015) 2545–2553, https://doi.org/10.1149/ma2015-03/1/364

[103] B. Wang, L. Bi, X.S. Zhao, Exploring the role of NiO as a sintering aid in BaZr0.1Ce0.7Y0.2O3-δ electrolyte for proton-conducting solid oxide fuel cells, J. Power Sources 399 (2018) 207–214, https://doi.org/10.1016/j.jpowsour.2018.07.087

[104] J.S. Park, J.H. Lee, H.W. Lee, B.K. Kim, Effects of ZnO addition methods on proton conductivities of barium zirconate modified by ytterbium, Solid State Ion. 224 (2012) 1–5, https://doi.org/10.1016/j.ssi.2012.07.005

[105] A.K. Baral, Reduction in sintering temperature of stable proton conductor BaCe0.35Zr0.5Y0.15O3-δ prepared by sol-gel method and its transport properties, Solid State Ion. 272 (2015) 107–111, https://doi.org/10.1016/j.ssi.2015.01.005

[106] K.-R. Lee, C. Tseng, S. Jang, J. Lin, K. Wang, J. Chang, T. Chen, S. Lee, Fabrication of anode-supported thin BCZY electrolyte protonic fuel cells using NiO sintering aid, Int. J. Hydrog. Energy 44 (2019) 23784–23792, https://doi.org/10.1016/j.ijhydene.2019.07.097

[107] C. Peng, J. Melnik, J. Li, J. Luo, A.R. Sanger, K.T. Chuang, ZnO-doped BaZr0.85Y0.15O3-δ proton-conducting electrolytes: characterization and fabrication of thin films, J. Power Sources 190 (2009) 447–452, https://doi.org/10.1016/j.jpowsour.2009.01.020

[108] M.M. Liu, Y. Liu, L. Yang, M.M. Liu, Z. Tang, Enhanced sinterability of BaZr0.1Ce0.7Y 0.1Yb0.1O3-δ by addition of nickel oxide, J. Power Sources 196 (2011) 9980–9984, https://doi.org/10.1016/j.jpowsour.2011.08.047

[109] D. Gao, R. Guo, Structural and electrochemical properties of yttrium-doped barium zirconate by addition of CuO, J. Alloy. Compd. (2010), https://doi.org/10.1016/j.jallcom.2009.12.082

[110] Z. Sun, E. Fabbri, L. Bi, E. Traversa, Lowering grain boundary resistance of BaZr0.8Y 0.2O3-δ with LiNO3 sintering-aid improves proton conductivity for fuel cell operation, Phys. Chem. Chem. Phys. 13 (2011) 7692–7700, https://doi.org/10.1039/c0cp01470b

[111] D. Han, K. Goto, M. Majima, T. Uda, Proton conductive BaZr0.8-xCexY0.2O3-δ: influence of NiO sintering additive on crystal structure, hydration behavior, and conduction properties, ChemSusChem 14 (2021) 614–623, https://doi.org/10.1002/cssc.202002369

[112] C. Duan, R.J. Kee, H. Zhu, C. Karakaya, Y. Chen, S. Ricote, A. Jarry, E.J. Crumlin, D. Hook, R. Braun, N.P. Sullivan, R. O'Hayre, Highly durable, coking and sulfur tolerant, fuel-flexible protonic ceramic fuel cells, Nature 557 (2018) 217–222, https://doi.org/10.1038/s41586-018-0082-6

[113] Z. Liu, M. Chen, M. Zhou, D. Cao, P. Liu, W. Wang, M. Liu, J. Huang, J. Shao, J. Liu, Multiple effects of iron and nickel additives on the properties of proton conducting yttrium-doped barium cerate-zirconate electrolytes for high-performance solid oxide fuel cells, ACS Appl. Mater. Interfaces 12 (2020) 50433–50445, https://doi.org/10.1021/acsami.0c14523

[114] S. Mu, H. Huang, A. Ishii, Z. Zhao, M. Zou, P. Kuzbary, F. Peng, K.S. Brinkman, H. Xiao, J. Tong, Rapid laser reactive sintering of BaCe0.7Zr0.1Y0.1Yb0.1O3-δ electrolyte for protonic ceramic fuel cells, J. Power Sources 4 (2020) 1–5.

[115] S. Nikodemski, J. Tong, C. Duan, R.O. Hayre, Ionic transport modification in proton conducting BaCe0.6Zr0.3Y0.1O3-δ with with transition metal oxide dopants, Solid State Ion. 294 (2016) 37–42, https://doi.org/10.1016/j.ssi.2016.06.020